Eur. Phys. J. A **19**, 11–23 (2004)
DOI 10.1140/epja/i2003-10106-3

THE EUROPEAN PHYSICAL JOURNAL A

Configuration-dependent bands in ^{169}Re

X.H. Zhou[1,a], M. Oshima[2], F.R. Xu[3], Y. Toh[2], Y.H. Zhang[1], Y. Zheng[1], Y.B. Xu[1], M. Koizumi[2], A. Osa[2], T. Hayakawa[2], Y. Hatsukawa[2], T. Shizuma[2], and M. Sugawara[4]

[1] Institute of Modern Physics, Chinese Academy of Sciences, Lanzhou 730000, PRC
[2] Japan Atomic Energy Research Institute, Tokai, Ibaraki 319-1195, Japan
[3] Department of Technical Physics and MOE Key Laboratory, Peking University, Beijing 100871, PRC
[4] Chiba Institute of Technology, Narashino, Chiba 275-0023, Japan

Received: 9 May 2003 /
Published online: 18 December 2003 –
Communicated by G. Orlandini

Abstract. High-spin states in ^{169}Re were studied and resulted in the identification of a strongly coupled band based on the $9/2^-[514]$ Nilsson state and a decoupled band built on the $h_{9/2}$ $1/2^-[541]$ intruder proton orbit. The cranked-shell-model calculations present configuration-dependent deformations that can explain the different band crossing frequencies. The $9/2^-[514]$ band in ^{169}Re shows the largest signature splitting at low spin among the known odd-mass Re isotopes. After the alignment of a pair of $i_{13/2}$ neutrons, the phase of the splitting is inverted with a significantly reduced amplitude. For the $9/2^-[514]$ bands in light odd-A Re isotopes, the signature splitting of the Routhians and its relation with the signature dependence of $M1$ transition matrix elements are investigated in connection with the deviation of nuclear shape from axial symmetry, suggesting an appreciable negative γ deformation for the very neutron-deficient odd-A Re isotopes. Additionally, a three-quasipariticle band was observed and assigned to be built likely on the $\pi 9/2^-[514] \otimes$ AE configuration.

PACS. 21.10.Re Collective levels – 23.20.-g Electromagnetic transitions – 23.20.Lv γ transitions and level energies – 27.70.+q $150 \leq A \leq 189$

1 Introduction

The systematic study of odd-Z nuclei can provide specific information about the influence of neutron shell fillings on the nuclear level structure. Nuclear shapes can be strongly dependent on configurations and neutron numbers. These changes can be particularly dramatic in the mass 170 region [1–9]. The very neutron-deficient odd-Z nuclei in the mass 170 region are located on the outer edge of the deformed rare-earth nuclei. These nuclei are expected to be rather soft with respect to β and γ deformations. Therefore, the shape-polarizing effects of individual nucleons can be significant [1–9]. For light odd-A Re isotopes, the proton Fermi surface is near the top of the $h_{11/2}$ and $d_{5/2}$ subshells; a small prolate deformation is favored when the $9/2^-[514]$ and $5/2^+[402]$ orbitals are filled [7–9]. The strongly down-sloping, deformation-driving $h_{9/2}$ $1/2^-[541]$ and $i_{13/2}$ $1/2^+[660]$ intruder orbitals are also close by. The odd proton in these orbitals may cause a much larger prolate deformation than the yrast or yrare $9/2^-[514]$ and $5/2^+[402]$ configurations [7–9]. Therefore, the $i^2_{13/2}$ neutron crossing should be delayed to higher frequencies, and lower alignment is associated with these low-Ω bands. By increasing deformation, the neutron Fermi surface is moved farther from the low-Ω components of the $\nu i_{13/2}$ subshell, thereby reducing the Coriolis mixing. This results in a decreased alignment gain and a higher crossing frequency associated with the alignment of $i_{13/2}$ neutrons [10]. In this paper, it is our aim to extend the high-spin level structure in odd-A Re isotopes to the very neutron-deficient nucleus ^{169}Re, and to study the dependence of band crossing frequencies, aligned angular momenta and signature splittings on the occupation of the different proton states and the neutron number.

Another interesting phenomenon concerns the occurrence of γ softness associated with the $9/2^-[514]$ bands, which were observed systematically in the rare-earth mass region [1–9]. The $9/2^-[514]$ bands are based on an $h_{11/2}$ spherical-shell-model state and have a large value of the magnetic-dipole transition operator. The decay sequences are characterized by mixed $M1/E2$ transitions which connect the two signatures of the band and compete with stretched $E2$ transitions within each signature decay sequence. One of the striking phenomena associated with these $9/2^-[514]$ bands is that they show unexpectedly

[a] e-mail: zxh@impcas.ac.cn

large signature splitting at low spins, whose amplitude increases considerably with decreasing neutron number to $N \sim 90$ [1–6]. However, after the first backbending (which is attributed to the rotational alignment of a pair of $i_{13/2}$ neutrons), the signature splitting has been observed to disappear or become inverted [1–9]. Cranked-shell-model calculations of quasiproton energies as a function of triaxial (γ) deformation [11,12] predict that the occupation of an orbit in the upper half of the $\pi h_{11/2}$ shell tends to drive the nucleus towards negative γ deformation, leading to an apparent signature splitting at low frequencies. At higher frequencies, the alignment of $i_{13/2}$ neutrons favors shapes with positive γ values [13–15]. The observed disappearance or inversion of signature splitting after the $i_{13/2}$ neutron alignment might indicate that the opposite γ driving forces of the strongly coupled proton and the aligned $i_{13/2}$ neutrons may cancel each other to some extent or even result in positive γ deformation. Although it is very difficult to find conclusive experimental evidence for the existence of a negative γ–deformed shape, such a suggestion has been made for the $9/2^-[514]$ bands in the light Lu and Ta isotopes [1–6]. This observation was based on signature splittings of the Routhians, $M1$ transition matrix elements, and the relation between them in connection with the triaxial (γ) deformation [1–6]. The high-spin level structure in the most neutron-deficient rhenium isotope investigated to date, ^{169}Re, combined with the available spectroscopic results of the other heavier odd-A Re isotopes [7–9,16], provides us with an opportunity to investigate the evolution of triaxial deformation in neutron-deficient Re isotopes with decreasing the neutron number.

Prior to this work, little information on the excited levels and band structure in ^{169}Re was available. The ground state of ^{169}Re was assigned to be the $\pi 9/2^-[514]$ Nilsson configuration [17]. In ^{173}Ir α-decay studies, the α-γ coincidence measurement revealed a 136 keV γ-ray which was proposed to depopulate the $11/2^-$ member of the $9/2^-[514]$ band in ^{169}Re [18]. Rotational bands in ^{169}Re were first reported in a conference proceeding [19], but a high-spin level scheme has not yet been published in the literature. Also, preliminary results of this investigation have been reported in ref. [20]

In this article, we report experimental results on high-spin band structures in ^{169}Re. The experimental details and data analyses will be described in sect. 2. The experimental quantities in the rotating frame and the theoretical calculations to understand the observed properties are presented in sects. 3 and 4, respectively. In sect. 5, the configuration assignments to the rotational bands are suggested on the basis of the measured in-band $B(M1)/B(E2)$ ratios, the existing knowledge of band properties in neighboring odd-proton nuclei, and the possible Nilsson states available for $Z = 75$ at a prolate deformation; band properties of the neutron AB crossing frequencies, alignment gains, and signature splittings are discussed with an emphasis on the nuclear-shape deviation from an axial symmetry associated with the $9/2^-[514]$ configuration in the very light odd-A Re nuclei. Concluding remarks are presented in sect. 6.

2 Experiments and results

2.1 Measurements

The excited states in ^{169}Re were populated via the ^{144}Sm (^{28}Si, $1p2n$)^{169}Re reaction. The ^{28}Si beam was provided by the tandem accelerator at the Japan Atomic Energy Research Institute (JAERI). The target was an isotopically enriched ^{144}Sm metallic foil of 1.3 mg/cm^2 thickness with a 7.0 mg/cm^2 Pb backing. The GEMINI [21] γ-ray detector array was used. At the time of this experiment, an array consisting of 12 HPGe's with BGO anti-Compton (AC) shields was used; six detectors had an efficiency of 40% each and the others had 70% relative to $3'' \times 3''$ NaI. The detectors were calibrated with ^{60}Co, ^{133}Ba, and ^{152}Eu standard sources; the typical energy resolution was about 2.0–2.4 keV at FWHM for the 1332.5 keV line.

To determine the optimum beam energy to produce ^{169}Re and to identify the in-beam γ-rays belonging to ^{169}Re, relative γ-ray yields were measured at beam energies of 150, 145, and 140 MeV. The 136 keV γ-ray was assigned to ^{169}Re previously [18]. The yield of the 136 keV γ-ray of ^{169}Re was maximized at a beam energy of 145 MeV, so this energy was used in the remainder of the experiment to populate high-spin states in ^{169}Re. Due to the neutron deficiency of the compound nucleus ^{172}Os, many reaction channels, such as $3n, 4n, 1p2n, 1p3n, 2p1n, 2p2n$,and $\alpha 2n$, were opened for the present projectile and target combination, which, together with γ-rays from EC/β^+-decay of the produced nuclei, yielded a complex γ-singles spectrum. Therefore, γ-γ-t and X-γ-t coincidences were examined. Here, t refers to the relative time difference between any two coincident γ-rays detected within $\pm$200 ns. A total of 250×10^6 coincidence events were accumulated. After accurate gain matching, these coincidence events were sorted into a symmetric total matrix for off-line analysis.

To obtain the DCO (Directional Correlations of γ-rays de-exciting the Oriented states) ratios, the detectors were divided into 3 groups positioned at 32° (148°), 58° (122°), and 90° with respect to the beam direction. A non-symmetrized matrix with detectors at $\theta_2 = 90°$ against those at $\theta_1 = 32°$ (and $\pm 148°$) was constructed. The experimental DCO ratio was calculated by $R_{\rm DCO}(\gamma) = I_\gamma(\theta_1)/I_\gamma(\theta_2)$, where $I_\gamma(\theta_1)$ represents the intensities of an unknown γ-ray along the θ_1-axis in coincidence with the stretched $E2$ transitions along the θ_2-direction. Similarly, with the same gates on the θ_1-axis, coincidence spectra along the θ_2-axis were projected to determine $I_\gamma(\theta_2)$. In the present geometry, stretched quadrupole transitions were adopted if $R_{\rm DCO}(\gamma)$ ratios were close to unity, and dipole transitions were assumed if $R_{\rm DCO}(\gamma) \leq 0.7$. Additionally, in order to extract information concerning γ-ray anisotropies, the coincidence data were sorted into two asymmetric matrices whose x-axis was the γ-ray energy deposited in the detectors at any angles and the y-axis was the γ-ray energy deposited in the detectors at 32° and 90°, respectively. By gating on the x-axis with suitable γ-rays, two spectra measured at 32° and 90° angle positions were obtained. After correcting for the overall detection efficiency of the detectors at each of the

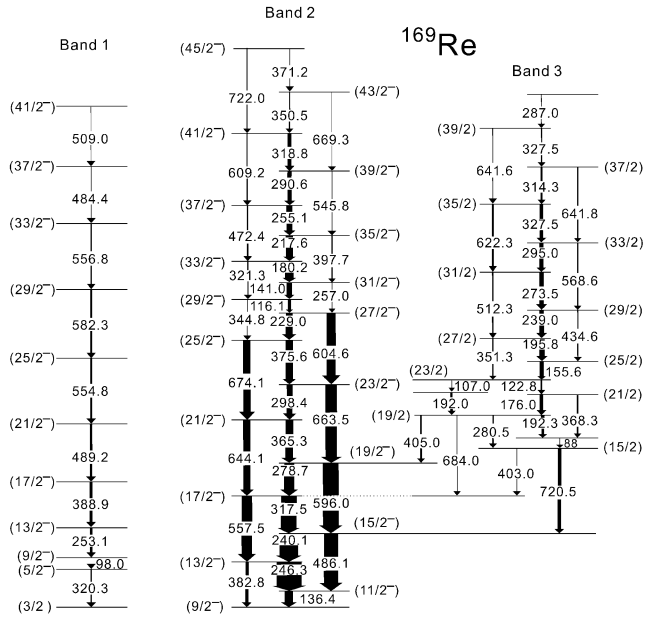

Fig. 1. Level scheme of ^{169}Re deduced from the present work. The widths of the arrows indicate the relative transition intensities.

two angles and normalizing the two spectra with respect to each other, γ-ray anisotropy ($R_{\rm ADO}(\gamma)$) was deduced from the intensity ratio in the two spectra. Typical γ-ray anisotropies for the known γ-rays observed in this experiment were 1.3 for stretched quadrupole transitions and 0.7 for stretched pure dipole transitions. Therefore, we assigned the stretched quadrupole transition and stretched dipole transition to the γ-rays of ^{169}Re with anisotropies around 1.3 and 0.7, respectively.

2.2 Level scheme

Since the nucleus ^{169}Re is very neutron deficient, there were many competing evaporation channels open in the present reaction, among which ^{168}W, ^{169}W and ^{169}Re were most strongly populated. The measured relative γ-ray yields at different beam energies, combined with Re K X-ray coincident information, helped us assign γ-ray cascades to ^{169}Re. The level scheme of ^{169}Re, including three rotational bands, is proposed from the present work as shown in fig. 1. The ordering of transitions in each band is determined according to the γ-ray relative intensities, γ-γ coincidence relationships and γ-ray energy sums. The transition character is deduced from the measured DCO and γ-ray anisotropy results. Since we do not have any direct measurement of the spins and parities for the states observed, the band head assignments rely merely on the existing knowledge of band properties in neighboring odd-Z nuclei and the possible Nilsson states available for $Z = 75$ at a prolate deformation. The configuration assignments to the bands will be discussed in sect. 5.

Band 1 has a typical character of decoupled band. A γ-ray spectrum gated on the 320.3 keV transition is

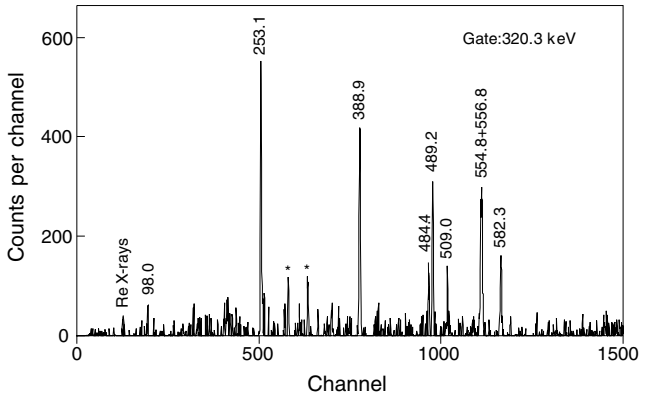

Fig. 2. The γ-ray spectrum gated on the 320.3 keV transition. The * symbols indicate contaminations.

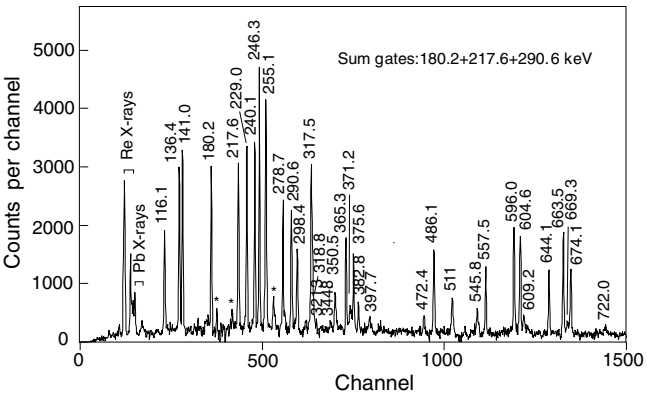

Fig. 3. Representative spectrum illustrating band 2 from a sum of gates as indicated on the panel. The * symbols indicate contaminations.

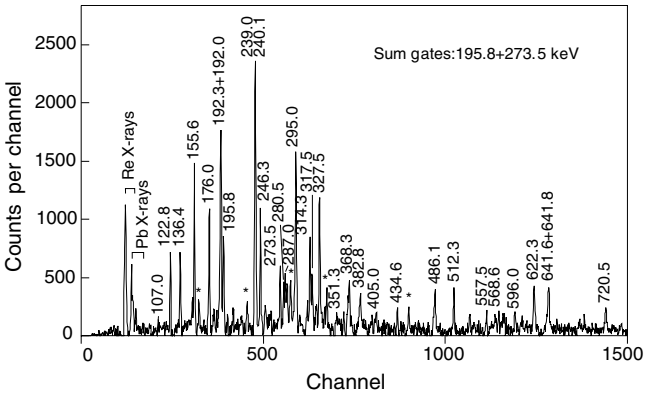

Fig. 4. Representative spectrum illustrating band 3 from a sum of gates as indicated on the panel. The * symbols indicate contaminations.

shown in fig. 2. The measured anisotropy shows that the 320.3 keV γ-ray is a stretched dipole transition. The lowest state of this band is most likely the state depopulated by the 320.3 keV line. The 98 keV transition was observed very weakly because of its highly converted nature and low detection efficiency. Angular correlations and anisotropies for transitions in the cascade above the proposed band head are consistent with the $\Delta I = 2$ character.

The transitions above the 320.3 keV transition are in coincidence with the 136.4 keV line which is believed to decay to the ground state, but the linking transitions were too weak to be observed. Its excitation energy could therefore not be determined.

Gated spectra demonstrating the existence of band 2 and band 3 are shown in figs. 3 and 4, respectively. Band 2 was populated most strongly, and the order of transitions is fixed firmly with the help of inter-band transitions. Band 2 arises presumably from the $\pi 9/2^-[514]$ Nilsson orbit, which is suggested by the α-γ coincidence measurement in ^{173}Ir α-decay study [18]. There are difficulties in establishing band 3 and the linking transitions to band 2 due to several doublets and low-energy transitions. The doublets of 327 and 641 keV, and the 239.0 keV transition which is overlapped by the 240.1 keV line depopulating the $15/2^-$ member of band 2, have been placed into band 3. Additionally, the doublet of 192 keV is proposed to exist in the linking transitions between band 2 and band 3. Justifications for the existence of these doublets come from the coincidence relationships, for example, the 192, 327 and 239 keV transition being in coincidence with another transition at the same energy. Furthermore, transitions near the top of band 3 (*i.e.* the 327 and 239 keV transitions) are nearly twice as strong as expected for a single transition.

2.3 Experimental transition probabilities

For the $\Delta I = 1$ rotational bands shown in fig. 1, the branching ratios, which are defined as

$$\lambda = \frac{T_\gamma(I \to I-2)}{T_\gamma(I \to I-1)} \tag{1}$$

were extracted for most transitions. Here $T_\gamma(I \to I-2)$ and $T_\gamma(I \to I-1)$ are the γ-ray intensities of the $\Delta I = 2$ and $\Delta I = 1$ transitions, respectively. These intensities are measured in a summed coincidence spectrum gated by the transitions above the state of interest. The branching ratios were used to extract the reduced transition probability ratios, which are defined as [22]

$$\frac{B(M1; I \to I-1)}{B(E2; I \to I-2)} = 0.697 \frac{[E_\gamma(I \to I-2)]^5}{[E_\gamma(I \to I-1)]^3} \frac{1}{\lambda} \frac{1}{1+\delta^2} \left(\frac{\mu_N^2}{e^2 b^2}\right), \tag{2}$$

where δ is the $E2/M1$ mixing ratio for the $\Delta I = 1$ transitions, and $E_\gamma(I \to I-1)$ and $E_\gamma(I \to I-2)$ are the $\Delta I = 1$ and $\Delta I = 2$ transition energies, respectively. The mixing ratio δ deduced from angular-correlation coefficients in the heavier odd-A Re isotopes varies between 0.0 and 0.2 [7–9]. This small value has little effect on the extracted reduced transition probability ratios. Consequently, the value $\delta = 0.0$ has been used in the present analysis.

The relative intensities for some uncontaminated γ-rays could be measured in the total projection spectrum. Most of the relative intensities were extracted from the spectra gated on the bottom transitions in the band.

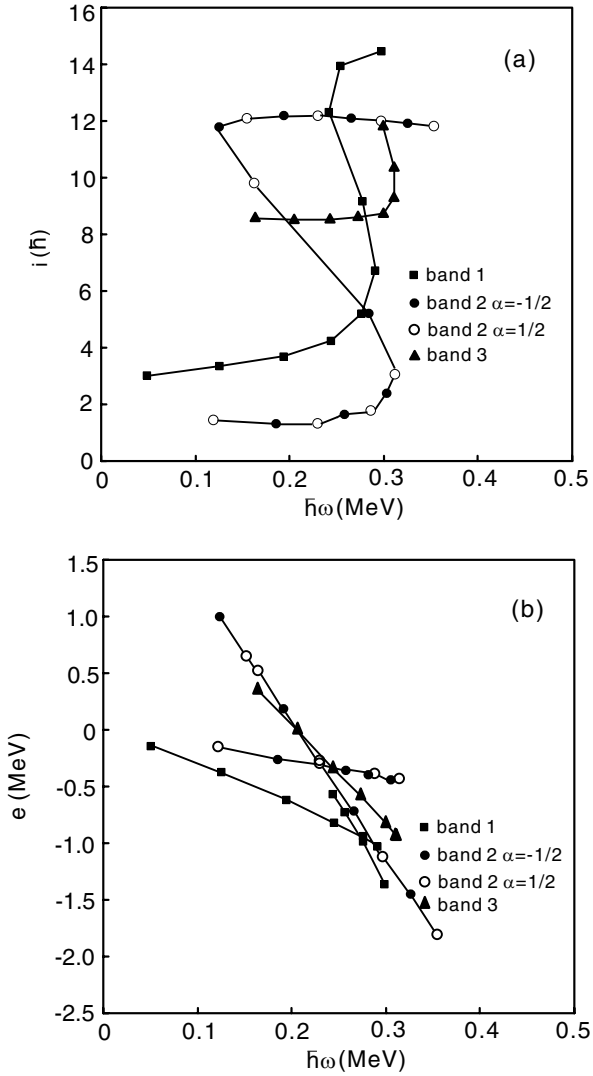

Fig. 5. Extracted alignment and Routhian energy for measured rotational bands in ^{169}Re (panels (a) and (b), respectively). The labels in the legends indicate the bands as they are labeled in fig. 1. The Harris reference parameters are chosen to be $J_0 = 20\hbar^2\,\mathrm{MeV}^{-1}$ and $J_1 = 60\hbar^4\,\mathrm{MeV}^{-3}$.

For some weak or heavily contaminated γ-rays, only upper or lower limits are given based on their intensity balance. The relative intensities are corrected with the detection efficiencies. The γ-ray energies, spin and parity assignments, relative γ-ray intensities, branching ratios λ, extracted $B(M1)/B(E2)$ values, DCO ratios, and anisotropies ($R_{\mathrm{ADO}}(\gamma)$) are presented in table 1 grouped in sequences for each band.

3 Experimental Routhians and alignments

The cranked shell model (CSM) is very successful in describing high-spin features like band crossing frequencies, rotational aligned angular momenta and signature splittings of many nuclei. In order to study the effect of rotation on the single-particle motion and compare the

Table 1. γ-ray transition energies, spin and parity assignments, γ-ray intensities, branching ratios, extracted $B(M1)/B(E2)$ ratios, DCO ratios, and γ-ray anisotropies in ^{169}Re.

E_γ(keV) [a]	$J_i^\pi \rightarrow J_f^\pi$ [b]	I_γ [c]	λ [d]	$B(M1)/B(E2)$ [e]	$R_{\rm DCO}$	$R_{\rm ADO}$
		Band 1				
98.0	$(\frac{9}{2}^-) \rightarrow (\frac{5}{2}^-)$	5			[g]	[g]
253.1	$(\frac{13}{2}^-) \rightarrow (\frac{9}{2}^-)$	30			0.96(15)	1.24(10)
388.9	$(\frac{17}{2}^-) \rightarrow (\frac{13}{2}^-)$	35			1.02(15)	1.32(10)
489.2	$(\frac{21}{2}^-) \rightarrow (\frac{17}{2}^-)$	31			1.06(15)	1.18(10)
554.8	$(\frac{25}{2}^-) \rightarrow (\frac{21}{2}^-)$	26			1.01(15)	1.32(10)
582.3	$(\frac{29}{2}^-) \rightarrow (\frac{25}{2}^-)$	22			0.97(15)	1.18(10)
556.8	$(\frac{33}{2}^-) \rightarrow (\frac{29}{2}^-)$	16			1.03(20)	1.36(20)
484.4	$(\frac{37}{2}^-) \rightarrow (\frac{33}{2}^-)$	12			1.04(20)	1.20(20)
509.0	$(\frac{41}{2}^-) \rightarrow (\frac{37}{2}^-)$	7			0.92(20)	1.12(20)
		Decay out transitions of band 1				
320.3	$(\frac{5}{2}^-) \rightarrow (\frac{3}{2})$	17			0.58(15)	0.71(10)
		Band 2				
136.4	$(\frac{11}{2}^-) \rightarrow (\frac{9}{2}^-)$	100			0.89(15)	1.08(10)
382.8	$(\frac{13}{2}^-) \rightarrow (\frac{9}{2}^-)$	38	0.13(02)	3.02(60)	0.99(15)	1.08(10)
246.3	$(\frac{13}{2}^-) \rightarrow (\frac{11}{2}^-)$	302			0.81(15)	0.86(10)
486.1	$(\frac{15}{2}^-) \rightarrow (\frac{11}{2}^-)$	187	0.90(18)	11(31)	1.03(15)	1.19(10)
240.1	$(\frac{15}{2}^-) \rightarrow (\frac{13}{2}^-)$	218			0.69(15)	0.76(10)
557.5	$(\frac{17}{2}^-) \rightarrow (\frac{13}{2}^-)$	125	0.68(14)	1.72(36)	1.01(15)	1.25(10)
317.5	$(\frac{17}{2}^-) \rightarrow (\frac{15}{2}^-)$	190			0.66(20)	0.68(20)
596.0	$(\frac{19}{2}^-) \rightarrow (\frac{15}{2}^-)$	189	1.79(36)	1.35(27)	1.04(15)	1.18(10)
278.7	$(\frac{19}{2}^-) \rightarrow (\frac{17}{2}^-)$	110			0.60(15)	0.66(10)
644.1	$(\frac{21}{2}^-) \rightarrow (\frac{17}{2}^-)$	89	1.04(20)	12(30)	1.08(15)	1.34(10)
365.3	$(\frac{21}{2}^-) \rightarrow (\frac{19}{2}^-)$	91			0.56(15)	0.67(10)
663.5	$(\frac{23}{2}^-) \rightarrow (\frac{19}{2}^-)$	150	2.213(44)	12(27)	0.99(15)	1.19(10)
298.4	$(\frac{23}{2}^-) \rightarrow (\frac{21}{2}^-)$	74			0.55(15)	0.64(10)
674.1	$(\frac{25}{2}^-) \rightarrow (\frac{21}{2}^-)$	93	1.22(25)	11(33)	1.01(15)	1.29(10)
375.6	$(\frac{25}{2}^-) \rightarrow (\frac{23}{2}^-)$	85			0.57(15)	0.62(10)
604.6	$(\frac{27}{2}^-) \rightarrow (\frac{23}{2}^-)$	110	1.22(29)	3.86(78)	1.06(15)	1.21(10)
229.0	$(\frac{27}{2}^-) \rightarrow (\frac{25}{2}^-)$	85			0.60(15)	0.67(10)
344.8	$(\frac{29}{2}^-) \rightarrow (\frac{25}{2}^-)$	≤ 10	≤ 0.30	$\geq 7.2(150)$	[g]	[g]
116.1	$(\frac{29}{2}^-) \rightarrow (\frac{27}{2}^-)$	30			0.66(15)	0.67(10)
257.0	$(\frac{31}{2}^-) \rightarrow (\frac{27}{2}^-)$	≤ 7	≤ 0.10	$\geq 2.78(60)$	[g]	[g]
141.0	$(\frac{31}{2}^-) \rightarrow (\frac{29}{2}^-)$	65			0.68(15)	0.70(10)
321.3	$(\frac{33}{2}^-) \rightarrow (\frac{29}{2}^-)$	13	0.10(2)	4.07(84)	0.97(20)	1.20(20)
180.2	$(\frac{33}{2}^-) \rightarrow (\frac{31}{2}^-)$	101			0.65(15)	0.71(10)
397.7	$(\frac{35}{2}^-) \rightarrow (\frac{31}{2}^-)$	21	0.33(10)	2.24(44)	0.96(20)	1.14(20)
217.6	$(\frac{35}{2}^-) \rightarrow (\frac{33}{2}^-)$	77			0.54(15)	0.57(10)
472.4	$(\frac{37}{2}^-) \rightarrow (\frac{33}{2}^-)$	18	0.25(8)	3.95(81)	1.11(20)	1.48(20)
255.1	$(\frac{37}{2}^-) \rightarrow (\frac{35}{2}^-)$	73			0.52(15)	0.54(10)
545.8	$(\frac{39}{2}^-) \rightarrow (\frac{35}{2}^-)$	15	0.38(11)	3.62(75)	1.06(20)	1.34(20)
290.6	$(\frac{39}{2}^-) \rightarrow (\frac{37}{2}^-)$	47			0.57(15)	0.55(10)
609.2	$(\frac{41}{2}^-) \rightarrow (\frac{37}{2}^-)$	12	0.35(10)	5.10(101)	1.07(20)	1.24(20)
318.8	$(\frac{41}{2}^-) \rightarrow (\frac{39}{2}^-)$	36			0.59(20)	0.64(20)
669.3	$(\frac{43}{2}^-) \rightarrow (\frac{39}{2}^-)$	[f]	0.50(20)	4.34(88)	0.99(20)	1.20(20)
350.5	$(\frac{43}{2}^-) \rightarrow (\frac{41}{2}^-)$	14			0.62(20)	0.67(20)
722.0	$(\frac{45}{2}^-) \rightarrow (\frac{41}{2}^-)$	10			[g]	[g]
371.2	$(\frac{45}{2}^-) \rightarrow (\frac{43}{2}^-)$	[f]			[g]	[g]

Table 1. Continued.

E_γ(keV) [a]	$J_i^\pi \rightarrow J_f^\pi$ [b]	I_γ [c]	λ [d]	$B(M1)/B(E2)$ [e]	$R_{\rm DCO}$	$R_{\rm ADO}$
			Band 3			
155.6	$(\frac{25}{2}) \rightarrow (\frac{23}{2})$	49			0.83(15)	0.79(10)
351.3	$(\frac{27}{2}) \rightarrow (\frac{23}{2})$	15	0.24(06)	2.05(40)	0.93(20)	1.17(20)
195.8	$(\frac{27}{2}) \rightarrow (\frac{25}{2})$	65			0.79(15)	0.80(10)
434.6	$(\frac{29}{2}) \rightarrow (\frac{25}{2})$	16	0.27	2.91(60)	1.09(27)	1.17(20)
239.0	$(\frac{29}{2}) \rightarrow (\frac{27}{2})$	60			0.69(20)	0.71(20)
512.3	$(\frac{31}{2}) \rightarrow (\frac{27}{2})$	20	0.35(08)	3.44(70)	1.08(20)	1.24(20)
273.5	$(\frac{31}{2}) \rightarrow (\frac{29}{2})$	55			0.64(20)	0.70(20)
568.6	$(\frac{33}{2}) \rightarrow (\frac{29}{2})$	19	0.37(06)	4.34(85)	0.99(20)	1.14(20)
295.0	$(\frac{33}{2}) \rightarrow (\frac{31}{2})$	51			0.64(20)	0.69(20)
622.3	$(\frac{35}{2}) \rightarrow (\frac{31}{2})$	21			1.09(20)	1.15(20)
327.5	$(\frac{35}{2}) \rightarrow (\frac{33}{2})$	60			0.63(20)[h]	0.68(20)[h]
641.8	$(\frac{37}{2}) \rightarrow (\frac{33}{2})$	15			1.06(20)[h]	1.24(20)[h]
314.3	$(\frac{37}{2}) \rightarrow (\frac{35}{2})$	25			0.64(20)	0.60(20)
641.6	$(\frac{39}{2}) \rightarrow (\frac{35}{2})$	60			1.06(20)[h]	1.24(20)[h]
327.5	$(\frac{39}{2}) \rightarrow (\frac{37}{2})$	10			0.63(20)[h]	0.68(20)[h]
287.0		[f]			[g]	[g]
			Transitions between band 2 and band 3			
88.0	$\rightarrow (\frac{15}{2})$	[f]			[g]	[g]
107.0	$(\frac{23}{2}) \rightarrow$	[f]			[g]	[g]
122.8	$(\frac{23}{2}) \rightarrow (\frac{21}{2})$	25			0.63(15)	0.65(10)
176.0	$(\frac{21}{2}) \rightarrow (\frac{19}{2})$	45			0.58(15)	0.66(10)
192.0	$\rightarrow (\frac{19}{2})$	30			[g]	[g]
192.3	$(\frac{19}{2}) \rightarrow$	35			[g]	[g]
280.5	$(\frac{19}{2}) \rightarrow (\frac{15}{2})$	19			1.08(20)	1.19(20)
368.3	$(\frac{21}{2}) \rightarrow$	25			[g]	[g]
403.0	$(\frac{15}{2}) \rightarrow (\frac{17}{2}^-)$	[f]			[g]	[g]
405.0	$(\frac{19}{2}) \rightarrow (\frac{19}{2}^-)$	15			[g]	[g]
684.0	$(\frac{19}{2}) \rightarrow (\frac{17}{2}^-)$	[f]			[g]	[g]
720.5	$(\frac{15}{2}) \rightarrow (\frac{15}{2}^-)$	40			1.04(20)	1.17(20)

[a] Uncertainties between 0.1 and 0.5 keV.
[b] See text for details about the spin and parity assignments.
[c] Uncertainties between 5 and 30%. Normalized to the 136.4 keV transition.
[d] Branching ratio: $T_\gamma(I \rightarrow I-2)/T_\gamma(I \rightarrow I-1)$, $T_\gamma(I \rightarrow I-2)$ and $T_\gamma(I \rightarrow I-1)$ are the relative γ intensities of the $E2$ and $M1$ transitions depopulating the level I, respectively.
[e] Extracted from the branching ratios assuming $\delta^2 = 0$.
[f] Too weak to extract accurate intensities.
[g] Could not be determined due to poor statistics or contaminations.
[h] Unresolved doublet. The ratio is for total peak.

properties of the observed rotational bands to the results of CSM calculations, we must transform the experimental excitation energies and spins into the rotating frame [12]. The experimental quasiparticle alignment can be calculated by

$$i(\omega) = I_x(\omega) - I_{\rm ref}, \tag{3}$$

where $I_x(\omega)$ is the component of the total angular momentum of the band on the axis of rotation and $I_{\rm ref}$ is the total aligned angular momentum of a reference configuration, and

$$I_{\rm ref} = \omega J_0 + \omega^3 J_1, \tag{4}$$

$$I_x(\omega) = \sqrt{\left(I + \frac{1}{2}\right)^2 - K^2}, \tag{5}$$

$$\hbar\omega = \frac{E_{\rm f} - E_{\rm i}}{I_x(I_{\rm f}) - I_x(I_{\rm i})},$$

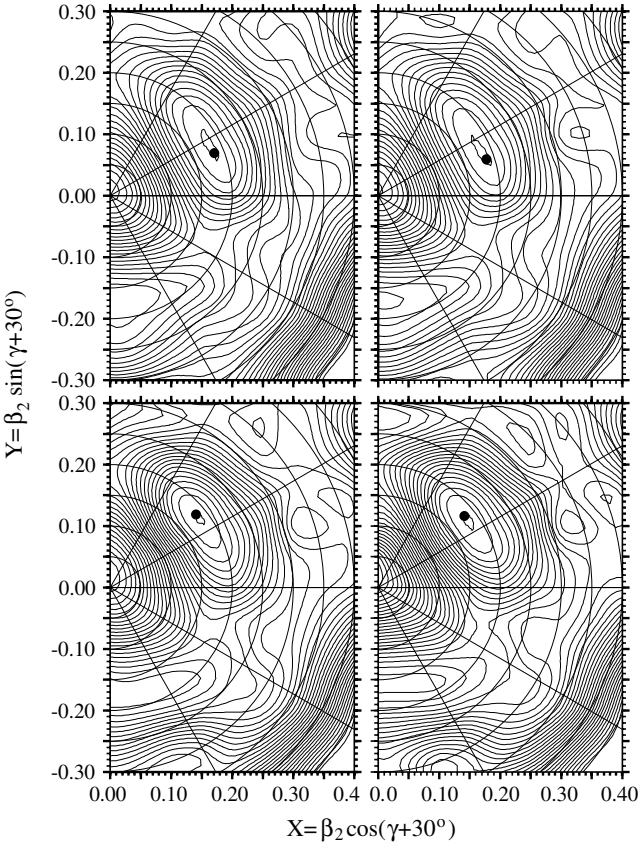

Fig. 6. Calculated Total Routhian Surfaces for the $(\pi, \alpha) = (-, -1/2)$ branch of band 2. The top left and top right panels correspond to $\hbar\omega = 0.10$ and 0.15 MeV (before the $i_{13/2}$ neutron alignment); the bottom left and bottom right panels correspond to $\hbar\omega = 0.25$ and 0.30 MeV (after the alignment). The energy difference between contours is 200 keV.

where J_0 and J_1 are the Harris parameters of the rotational reference configuration. It is difficult to choose a reference to be suitable for all of the bands in ^{169}Re since different quasiparticle excitations may change the deformation. We have chosen a reference given by the Harris parametrization $J_0 = 20\hbar^2\,\mathrm{MeV}^{-1}$ and $J_1 = 60\hbar^4\,\mathrm{MeV}^{-3}$, which give a good description to the yrast band in ^{168}W [23].

The experimental level energies $E(I)$ are transformed from the laboratory frame into the rotating frame $E(\omega)$ according to [12]

$$E(\omega) = E(I) - \hbar\omega I_x. \tag{6}$$

The Routhian e is obtained by subtracting a reference E_{ref} from $E(\omega)$. The reference energy E_{ref} is defined as

$$E_{\mathrm{ref}} = -\int I_{\mathrm{ref}}\mathrm{d}\omega = -\frac{1}{2}\omega^2 J_0 - \frac{1}{4}\omega^4 J_1 + \frac{1}{8}J_0. \tag{7}$$

The resulting calculations of quasiparticle alignment and Routhian energy for all bands observed in ^{169}Re are plotted *vs.* the rotational frequency in fig. 5.

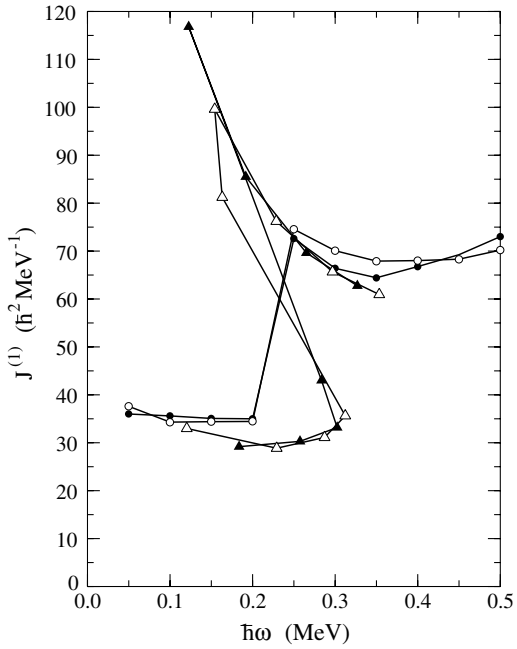

Fig. 7. Experimental and calculated moments of inertia for band 2. Filled and open triangles (circles) stand for the experimental (calculated) values of the $\alpha = -1/2$ and $\alpha = +1/2$ branches, respectively.

4 Theoretical calculations

In order to have a deeper understanding of the band structures in ^{169}Re, we have performed cranked-shell-model (CSM) calculations by means of the Total-Routhian-Surface (TRS) method [24] in the three-dimensional deformation β_2, β_4, γ space. The nonaxial deformed Woods-Saxon (WS) potential [25] was employed. Both monopole and quadrupole pairings [26,27] were included. To avoid the spurious pairing phase transition encountered in the BCS approach, we used the approximate particle number projection named Lipkin-Nogami pairing [28]. The pairing correlation is dependent on rotational frequency ($\hbar\omega$) and deformation. In order to include such dependence in the TRS, we have done pairing-deformation-frequency self-consistent TRS calculations, *i.e.*, for any given frequency and deformation, the pairing is self-consistently calculated by the HFB-like method [28]. At a given frequency, the deformation of a state is determined by minimizing the calculated TRS.

The TRS calculations show, for band 2, based on the $9/2^-[514]$ configuration, that the β_2 deformation is about 0.18 and a pair of $i_{13/2}$ neutrons align at $\hbar\omega \approx 0.22$ MeV. Figure 6 displays the calculated TRSs of the negative signature ($\alpha = -1/2$) branch of band 2 at $\hbar\omega = 0.10$, 0.15 MeV (before alignment) and $\hbar\omega = 0.25$, 0.30 MeV (after alignment). The calculated moment of inertia (J_1) is shown in fig. 7 in comparison with the experiment. The present self-consistent CSM works well only for yrast rotational states with a given parity and signature. This hinders us to do self-consistent cranked calculations for band 1 built on the $1/2^-[541]$ configuration that has

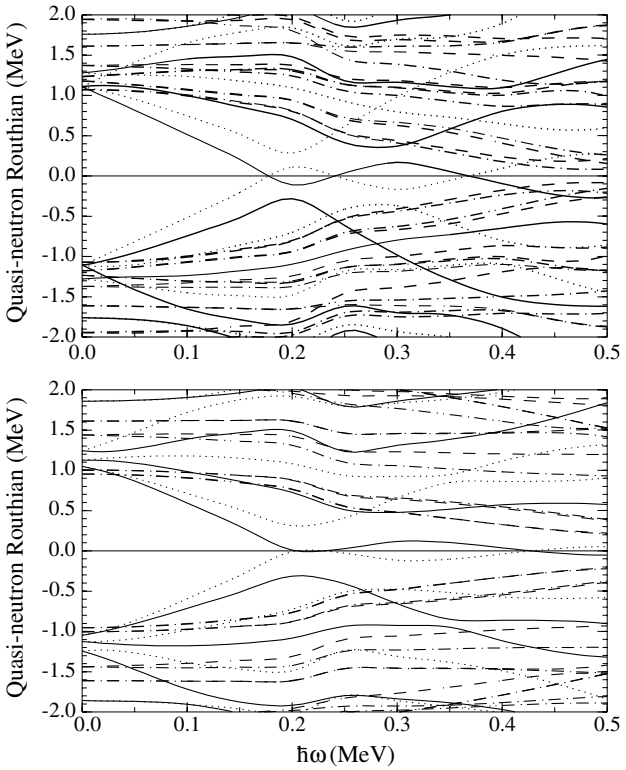

Fig. 8. Calculated quasineutron Routhians as a function of rotational frequency ($\hbar\omega$) in ^{169}Re. The upper panel was calculated with $\beta_2 = 0.18$ ($\beta_4 = 0$) corresponding to the case of band 2. The lower panel was done with $\beta_2 = 0.22$ ($\beta_4 = 0.026$) that is the calculated deformation of band 1. In both cases, $\gamma = 0°$. The parity and signature (π, α) of the Routhians are represented as follows: $(+, +1/2)$ solid lines, $(+, -1/2)$ dotted lines, $(-, +1/2)$ dash-dotted lines, and $(-, -1/2)$ dashed lines. The lowest neutron Routhians with $\alpha = +1/2$ and $-1/2$ are the $i_{13/2}$ orbitals.

higher energies but the same parity and signature as the $\alpha = +1/2$ branch of band 2. However, we did the configuration-constraint calculation [29] for the band head of band 1. It was calculated that band 1 has a larger deformation with $\beta_2 = 0.22$ ($\gamma = 0°$) compared with band 2. With the different deformations, we plotted quasineutron Routhians as shown in fig. 8. It can be seen that $i_{13/2}$ neutrons have a delayed alignment in band 1 (due to the larger β_2 deformation) and the alignment is sharper in band 2. These are consistent with the observations.

Mueller *et al.* have calculated the equilibrium deformations for ground states and intruder configurations in odd-A Re isotopes [30]. The calculations indicate that for ^{169}Re the deformation-aligned bands are expected to have quadrupole deformations around 0.18, while the rotational-aligned bands based on the $1/2^-[541]$ and $1/2^+[660]$ Nilsson orbits tend to have larger deformations [30]. These results are consistent with the present calculated deformations. Thus, the available Nilsson orbits for ^{169}Re at the predicted prolate deformations are the $1/2^+[411]$, $5/2^+[402]$, $7/2^+[404]$, $9/2^-[514]$, $1/2^-[541]$ and $1/2^+[660]$, among which the high-j orbits $9/2^-[514]$,

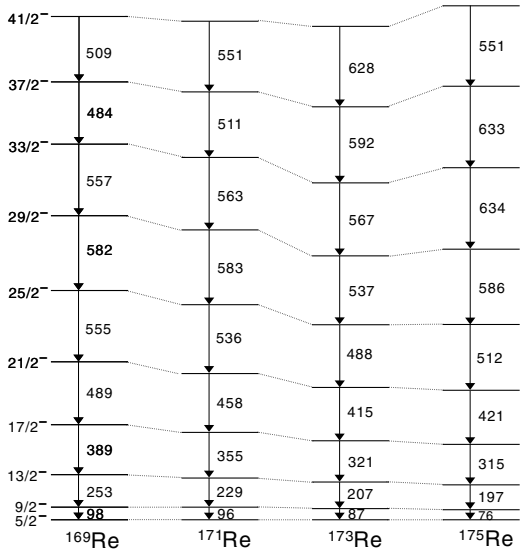

Fig. 9. Comparing the level spacings of band 1 with those of the $1/2^-[541]$ bands in $^{171-175}$Re.

$1/2^-[541]$ and $1/2^+[660]$ of the $h_{11/2}$, $h_{9/2}$ and $i_{13/2}$ parentages are particularly important for the high-spin states. The different orbits will give rise to rotational bands with different spectroscopic characters. When the high-Ω orbits are occupied, strongly coupled bands with strong $\Delta I = 1$ transitions will occur. The unpaired proton in the low-Ω orbits will, on the other hand, easily be decoupled and align their spins, and bands with large signature splittings would be observed. At high spins a pair of intruder high-j particles are expected to break up and align their angular momenta along the rotation axis producing an upbend or a backbend. In the mass region around ^{169}Re, the experimental results [1–9] and theoretical calculations as shown in fig. 8 have demonstrated that the aligned i_{13}^2 neutron configuration is responsible for the first band crossing.

5 Discussion

5.1 Band based on the $1/2^-[541]$ configuration

Band 1 has a decoupled structure, suggesting that the configuration includes a proton from an $\Omega = 1/2$ orbit. Candidate orbits are $1/2^+[411]$, $1/2^-[541]$ and $1/2^+[660]$. Figure 9 compares the level spacings of band 1 with those of the $1/2^-[541]$ bands in the heavier odd-A Re isotopes [7–9,16], indicating that band 1 follows the trends very well. As shown in fig. 2, the γ-rays in band 1 are in coincidence with Re K X-rays. Therefore, band 1 is assumed to be based on the $1/2^-[541]$ Nilsson orbital, with a band head spin and parity of $5/2^-$. This band has an alignment of approximately $3.5\hbar$ before the backbend (see fig. 5), in agreement with what is expected for an aligned proton state occupying the $1/2^-[541]$ orbit. The unfavored branch has not been observed because of its large signature splitting. As shown in fig. 5, the band crossing takes

place at $\hbar\omega = 0.27$ MeV, where the gain in the alignment is about $10.5\hbar$. The AB neutron crossing is delayed by about 40 keV in the decoupled band compared with the strongly coupled band. Similar shifts have been observed for the $1/2^-[541]$ bands in a large number of odd-Z nuclei in this mass region and can be qualitatively attributed to the larger quadrupole deformation for the $1/2^-[541]$ configuration [1–9], which has a negative slope in the Nilsson diagrams and thus drives the nucleus toward larger deformation. Theoretical CSM calculations predict that the quadrupole deformation β_2 values are 0.22 and 0.18 for the $1/2^-[541]$ and $9/2^-[514]$ configurations, respectively. Since the neutron Fermi level, λ_n, is above the highly alignable low-Ω $i_{13/2}$ neutron orbits, an increased deformation corresponds to an increased quasineutron energy, E_ν, for the $i_{13/2}$ quasineutron:

$$E_\nu = \sqrt{\Delta^2 + (\varepsilon_\nu - \lambda_\nu)^2}, \tag{8}$$

resulting in a delayed AB neutron band crossing [31]. Figure 8 displays that the neutron AB crossing frequency increases with increasing quadrupole deformation. By inspecting the alignment gains in the $1/2^-[541]$ bands caused by the first AB neutron crossing in the odd-A Re isotopes [7–9], it is found that the alignment gain is increased while decreasing the neutron number. By decreasing the neutron number, the neutron Fermi surface is moved closer to the low-Ω components of the $\nu i_{13/2}$ subshell, resulting in an increased gain in aligned angular momentum associated with the alignment of $i_{13/2}$ neutrons.

In the present work, the $1/2^-[541]$ band head energy in ^{169}Re was observed to be higher than 320 keV above the ground state, which might explain the low population for the $1/2^-[541]$ band in ^{169}Re compared with those in the heavier odd-A Re isotopes [7–9]. The low population of the $1/2^-[541]$ band in ^{169}Re is also supported in the calculations of Mueller, wherein the band head excitation energies of the $1/2^-[541]$ bands in the light Re isotopes are predicted to increase with decreasing neutron number, with the calculated excitation energy of the $1/2^-[541]$ configuration in ^{169}Re as high as 541 keV above the ground state [30].

5.2 Band based on the $9/2^-[514]$ configuration

Band 2 was most strongly populated and extended up to $(45/2^-)$. Considering the alignment, band crossing frequency, $B(M1)/B(E2)$ ratios, signature splitting, and level spacings, band 2 is presumed to be associated with the $9/2^-[514]$ configuration which was assigned to be the ground state of ^{169}Re. This configuration assignment is also supported by the α-decay studies of ^{173}Ir [18].

Band 2 experiences a strong backbending at $\hbar\omega = 0.23$ MeV with gain of $10.5\hbar$ in alignment (see fig. 5), corresponding well to the AB neutron crossing in the $9/2^-[514]$ bands of the neighboring odd-A Re isotopes [7–9]. The experimental neutron AB crossing frequency is well reproduced by the CSM calculation as shown in fig. 8. The TRS calculation shown in fig. 6 corresponds to this band, as it comprises the ground state. This configuration is γ soft at low rotational frequencies with potential minimum at $\beta_2 \sim 0.18$ and $\gamma \sim -10^\circ$. After the first band crossing the predicted nuclear shape is still γ soft with the energy minimum at about the same quadrupole deformation, but at small positive γ deformation.

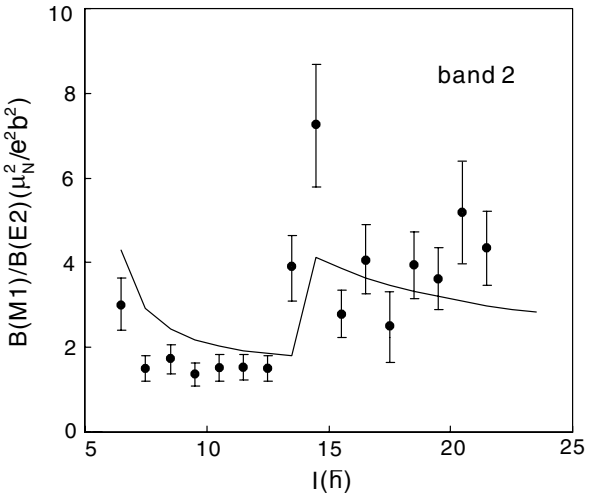

Fig. 10. Experimental $B(M1)/B(E2)$ ratios for the $9/2^-[514]$ band, and theoretical prediction assuming $\gamma = 0^\circ$ as described in the text.

Further information about the structure of the $9/2^-[514]$ band can be obtained by comparing theoretical $B(M1)/B(E2)$ values with experimental ones. The experimental $B(M1)/B(E2)$ ratios have been deduced according to eq. (2) described in the previous section. The experimental data is shown in fig. 10 together with theoretical estimates obtained from a semiclassical formula [32,33]:

$$\frac{B(M1; I \to I-1)}{B(E2; I \to I-2)} = \frac{12}{5Q_0^2 \cos^2(\gamma + 30^\circ)} \times \left[1 - \frac{K^2}{(I-1/2)^2}\right]^{-2} \frac{K^2}{I^2} \Big\{ (g_1 - g_R) \times [(I^2 - K^2)^{1/2} - i_1] - (g_2 - g_R) i_2 \Big\}^2 \left(\frac{\mu_N^2}{e^2 b^2}\right). \tag{9}$$

This expression takes into account the effect of triaxiality γ on $E2$ transition rate. The suffixes 1 and 2 refer to the strongly coupled and decoupled quasiparticles, respectively. The gyromagnetic g_1 and g_2 factors were taken from ref. [7], and the rotational gyromagnetic factor g_R was taken here as $Z/A = 0.443$. The alignment of the strongly coupled particle was set to $i_1 = 1.5\hbar$ and for the three-quasiparticle band a value $i_2 = 10.5\hbar$ as deduced from experiment was used for the decoupled neutron pair. The nominal band head K-value of 4.5 was used. The quadrupole moment was set to $Q_0 = 5.5$ eb, which corresponds to the quadrupole deformation of the even-even core nucleus ^{168}W [34]. By assuming $\gamma = 0^\circ$, the experimentally observed trend of $B(M1)/B(E2)$ ratios for the $9/2^-[514]$ band is reproduced by the theory if the alignment gain is attributed to the AB neutron crossing. At low

spin the theoretical values for $\gamma = 0°$ overestimate the experiment, and improved agreement could be obtained for negative γ deformation. The $B(M1)/B(E2)$ ratios for the $9/2^-[514]$ band show a pronounced increase of a factor of 2 at the spin where the alignment first reaches its maximum. The ratios of reduced transition probabilities at low spins and the increase after the backbending for the $9/2^-[514]$ band in ^{169}Re are comparable to those obtained in the $9/2^-[514]$ bands of the heavier Re isotopes [7,9]. In the theory, the increase in the $B(M1)/B(E2)$ ratios can result not only from an enhancement of the $B(M1)$ rate arising from the g-factor of the two aligned $i_{13/2}$ neutrons but also from a decrease in the $B(E2)$ rate due to the loss in collectivity as the γ deformation parameter shifts from negative values to small positive values. It is expected that a small change of the quadrupole moment affects the calculated ratios only slightly. Assuming a constant quadrupole moment, the experimentally observed increase in the $B(M1)/B(E2)$ ratios can be well reproduced by the model calculation if the origin of the backbend in the $9/2^-[514]$ band is proposed as the $i_{13/2}$ neutron alignment.

The observation of the $9/2^-[514]$ band in the most neutron-deficient rhenium isotope investigated to date, ^{169}Re, combined with the available spectroscopic results of the other light odd-A Re isotopes [7–9,16], provides us with an opportunity to investigate the evolution of triaxial deformation in neutron-deficient Re isotopes while decreasing the neutron number. In the following sections, we discuss the nuclear-shape deviation from an axial symmetry associated with the $9/2^-[514]$ configuration in very light odd-A Re nuclei on the basis of the signature splittings of the Routhians and $M1$ transition matrix elements and the relation between them in connection with the triaxial (γ) deformation.

5.2.1 Increasing signature splitting of the Routhians

For systems with odd-particle number, the signature defined by $\alpha_{\rm f} = 1/2(-1)^{j-1/2}$ (favored signature) is lowered in energy with respect to the $\alpha_{\rm u} = 1/2(-1)^{j+1/2}$ (unfavored) signature [35], where the angular momentum of the odd particle is expressed by j. The signature splitting Δe is defined as the difference in energies at a given rotational frequency for the pair of signature partners. Figure 11 presents plots of the signature splittings for the $9/2^-[514]$ bands in the light odd-A Re nuclei [7–9,16], defined as [36]

$$S(I) = [E(I) - E(I-1)] - \frac{1}{2} \times [E(I+1) - E(I) + E(I-1) - E(I-2)]\,. \quad (10)$$

Here $E(I)$ is the level energy of state I; $S(I)$ is directly proportional to the signature splitting Δe, but magnified by approximately a factor of two. There is a clear energy splitting between the two signatures at low frequencies, and after the $i_{13/2}$ neutron alignment the phase of signature splitting is inverted with a much reduced amplitude (see the insets of fig. 11). In the odd-A Re isotopes with

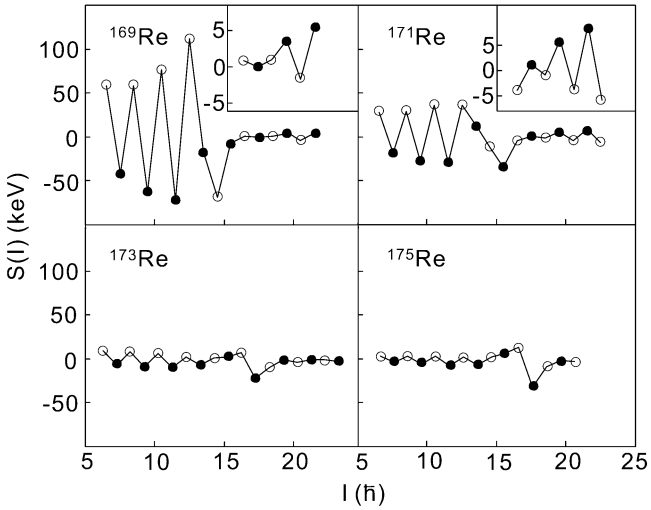

Fig. 11. Signature splitting $S(I)$ as a function of spin I for the $9/2^-[514]$ bands in $^{169-175}$Re. The filled and open symbols correspond to the favored and unfavored signatures, respectively.

mass number larger than 175, there is almost no signature splitting in the $9/2^-[514]$ bands [37]. As shown in fig. 11, the experimentally observed signature splitting in the very neutron-deficient isotopes is unexpectedly large, and increases rapidly with decreasing neutron number. A signature splitting as high as approximately 30 keV has been observed at low spins in ^{169}Re.

Signature splitting of the energies is considered generally as a consequence of the mixing of the $\Omega = 1/2$ orbits into the wave functions, due to the Coriolis interaction. Since the proton Fermi level lies high in the $h_{11/2}$ subshell in Re isotopes with a proton number of 75, the mixing of the $\Omega = 1/2$ components into the wave functions should be very small for an axially symmetric nuclear shape. A signature splitting does not necessarily imply a triaxial nuclear shape, but the magnitude of Δe could offer a clue for possible γ deformation. It is well known that the magnitude of signature splitting is expected to be very dependent on several properties such as the nuclear deformation, pairing, and shell filling [38]. For example, the decreasing nuclear quadrupole deformation β_2 can result in an increased signature splitting since in the lowest order Δe is proportional to $(\beta_2)^{-2\Omega+1}$ if pairing is neglected [38]. The increased signature splitting amplitudes for the lighter Re isotopes seem therefore to be explained in terms of the decreasing nuclear quadrupole deformation as indicated by the theoretical calculation [30]. However, changing the pairing gap, quadrupole deformation β_2, and hexadecapole deformation β_4 in large intervals, the particle-rotor and cranked-shell-model calculations adopting an axially symmetric nuclear shape show that the predicted magnitude of the signature splitting is nevertheless much less than the observed value in the neutron-deficient isotopes [3,7,15]. Thus, in order to reproduce the large signature splitting in the $9/2^-[514]$ bands in light Re isotopes, a mechanism leading to enhanced mixing with an $\Omega = 1/2$ orbit is needed. The rapid increase of signature

splitting with decreasing neutron number in the bands associated with the same quasiproton configuration strongly suggests that the observed trend is due to the nuclear-shape change of the even-even core. It seems reasonable to postulate that it is the enhanced nonaxially symmetric shape with decreasing the neutron number that causes the experimentally observed increasing signature splitting. Indeed, the TRS calculations as shown fig. 6 show energy minimum with negative γ deformation at low frequencies, and the increasing γ softness with decreasing neutron number for odd-A Re isotopes can also be predicted.

R. Bengtsson *et al.* [39] pointed out that the positive γ deformation may cause signature inversion in the configuration of $\pi h_{11/2} \otimes \nu i^2_{13/2}$, where the aligned neutrons could produce a positive γ deformation. After the $i_{13/2}$ neutron alignment, the predicted nuclear shape, as shown in fig. 6, is γ soft with the energy minimum at apparent positive γ deformation. Therefore, the observed inversion of signature splitting with small amplitude at high frequencies might indicate that the γ driving force of the aligned $i_{13/2}$ neutrons, favoring positive direction, is stronger than that of the strongly coupled $h_{11/2}$ proton favoring negative γ value, and this might result in a nuclear shape with small positive γ deformation.

5.2.2 Relative signature splitting of the $B(M1)/B(E2)$ ratios below the backbending

The $B(M1)/B(E2)$ ratios can exhibit a signature splitting, which is known to represent the splitting in the magnetic transition rates $\Delta B(M1)$ [4], where $\Delta B(M1)$ is the difference between the $B(M1{:}\alpha_{\rm f} \rightarrow \alpha_{\rm u})$ and $B(M1{:}\alpha_{\rm u} \rightarrow \alpha_{\rm f})$. It is believed that the $B(E2)$ values show smooth dependence on spin, and, in particular, do not exhibit signature dependence even in the case of triaxially deformed nuclear shapes [40]. Therefore, the relative signature splitting of the magnetic transition rates $\Delta B(M1)/\langle B(M1)\rangle$, where $\langle B(M1)\rangle$ is defined as $1/2[B(M1{:}\alpha_{\rm f} \rightarrow \alpha_{\rm u}) + B(M1{:}\alpha_{\rm u} \rightarrow \alpha_{\rm f})]$, can be expressed by the ratio of $\Delta[B(M1)/B(E2)]/\langle B(M1)/B(E2)\rangle$. According to a semiclassical approximation based on the cranking approach [41,33], we can obtain the following relationship:

$$\frac{\Delta[B(M1)/B(E2)]}{\langle B(M1)/B(E2)\rangle} = \frac{4[(1-K^2/I^2)^{1/2} - i_p/I] \times (\Delta e/\hbar\omega)}{[(1-K^2/I^2)^{1/2} - i_p/I]^2 + (\Delta e/\hbar\omega)^2}, \quad (11)$$

where i_p, K, I, Δe, and $\hbar\omega$ denote the quasiproton aligned angular momentum, band head K-value, angular momentum, energy signature splitting, and rotational frequency, respectively. It should be pointed out that the formula is valid only for axially symmetric nuclei, or it can give a reasonable description for nuclei with a slight deviation from axial symmetry. Assuming $i_p = 1.5\hbar$ and $K = 4.5$, the $\Delta B(M1)/\langle B(M1)\rangle$ values for the $9/2^-[514]$ bands in light odd-A Re isotopes were calculated by using the experimental values of Δe and $\hbar\omega$, and the results are presented in fig. 12. The experimental values extracted from eq. (2) and averaged in the low-spin region around $I = 17/2\hbar$ [7–9,16], also shown in fig. 12, remain almost constant for the nuclei in discussion. The calculated $\Delta B(M1)/\langle B(M1)\rangle$ values are consistent with the experimental ones for ^{173}Re and ^{175}Re, whereas apparent deviations appear while decreasing the neutron number. For ^{169}Re, the theoretical value is found to exceed the experimental one by a factor of about 4.0. The monotonic increase in the deviations between the experimental and calculated values of $\Delta B(M1)/\langle B(M1)\rangle$ with decreasing neutron number suggests increased triaxiality [1].

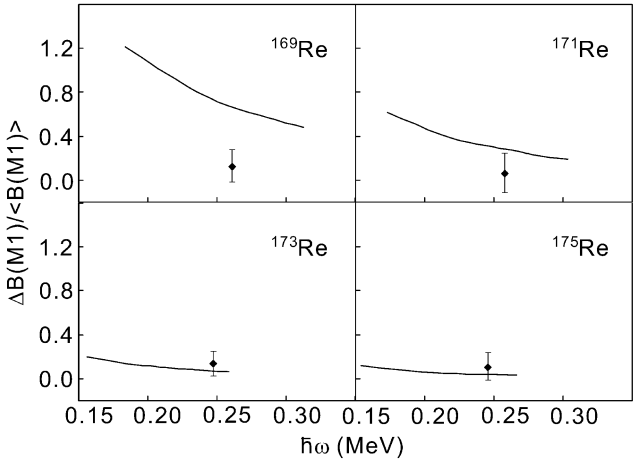

Fig. 12. $\Delta B(M1)/\langle B(M1)\rangle$ ratios shown as a function of rotational frequency for the $9/2^-[514]$ bands in $^{169-175}$Re. Also shown are the experimental relative signature splittings averaged around $I = 17/2\hbar$.

5.2.3 Relationship between the signature splittings of the Routhians and $B(M1)$ values

In order to investigate the deviation of nuclear shape from axial symmetry and the direction of γ deformation, theoretical studies revealed that for axially symmetric nuclear shapes a correlation between the signature splittings of the $B(M1)$ values and Routhians can be obtained as [42]

$$\frac{\Delta B(M1)}{\langle B(M1)\rangle} = \frac{4(\Delta e)(\hbar\omega)}{(\Delta e)^2 + (\hbar\omega)^2}. \quad (12)$$

This equation is exact for axially symmetric shapes in the cranking model for any cranking frequency $\hbar\omega$, and valid if $I \gg 1$ in the particle-rotor model for the one-quasiparticle deformation-aligned bands where K is a good quantum number. For negative γ deformations the left-hand side of the equation has a lower value than the right-hand side, and for positive γ deformation a higher value [42]. On the basis of such a comparison, it has been suggested that the neutron-deficient Ho, Tm, Lu, and Ta isotopes deviate appreciably ($-15^\circ \geq \gamma \geq -25^\circ$) from an axially symmetric

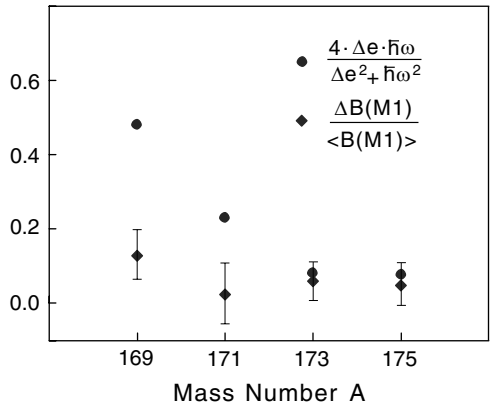

Fig. 13. Comparison between the quantities of the left- and right-hand sides of eq. (12).

shape [42]. Figure 13 compares the left- and right-hand side values of eq. (12) by choosing the data around $I = 17/2$ before the $i_{13/2}$ neutron alignment for the $9/2^-[514]$ bands in the light odd-A Re isotopes [7–9,16]. We remark that the quantities shown in fig. 13 are calculated by using the experimental observed Routhian splitting Δe and $B(M1)/B(E2)$ ratios. The increasing difference between the two sides with decreasing neutron number indicates a considerable negative γ deformation for ^{169}Re.

5.3 Band based possibly on the $\pi 9/2^-[514] \otimes$ AE configuration

As shown in fig. 5, band 3 has the largest aligned angular momentum with a value of about $8.5\hbar$ at low spins. The alignment was deduced by assuming a band head K-value of 4.5; the alignment in such high-spin levels is expected to be less influenced by the uncertainty of the K-value. This band shows an upbend at $\hbar\omega \approx 0.31$ MeV, and there is no signature splitting up to the highest level observed. In view of such a large alignment, band 3 is assumed to be based on a configuration of at least three quasiparticles. The band crossing frequency of $\hbar\omega \approx 0.31$ MeV is much higher than the AB neutron crossing in the neighboring nuclei [7,9,14, 43,44], indicating that band 3 involves an $i_{13/2}$ neutron. A one-quasiparticle occupation of the lowest $\nu i_{3/2}$ state would inhibit the normal $\nu i_{13/2}$ alignment from occurring at the expected rotational frequency. This well-known blocking effect can be seen in odd-N nuclei throughout the rare-earth region. Inspecting the level structure in the nuclei around ^{169}Re [23,14,43,44], we propose that band 3 is likely based on the $\pi 9/2^-[514] \otimes \nu$AE configuration. Here, A ($\pi = +$, $\alpha = +1/2$) and E ($\pi = -$, $\alpha = +1/2$) are the conventional cranked-shell-model orbits labelling the lowest configurations in the $\nu i_{13/2}$ and $\nu f_{7/2}h_{9/2}$ subshells [14], respectively. The A and E orbits were observed at very low excitation energies at the neighboring odd-N nuclei [23,43,14]; the AE configurations were also identified at excitation energies around 1.6 MeV in the neighboring even-even nuclei [23,14,43,44], which are comparable with the band head energy of band 3. Thus, the $\pi 9/2^-[514] \otimes \nu$AE configuration would be expected to be energetically favorable in ^{169}Re. Most of the alignment in band 3 would be contributed by the $\nu i_{13/2}$ quasiparticle, while the rest might be associated with the other two quasiparticles. The upbend at $\hbar\omega \approx 0.31$ MeV may be caused by the BC neutron alignment because the crossing frequency is similar to those for the BC neutron alignments observed in the nuclei around ^{169}Re [23,14,43,44].

6 Summary and conclusions

The odd-proton nucleus ^{169}Re has been produced in the bombardment of the ^{144}Sm target with the ^{28}Si projectiles. A level scheme consisting of three rotational bands has been established. The possible quasiparticle configurations of these bands have been suggested based on the measured in-band $B(M1)/B(E2)$ ratios and the existing knowledge of band structures in the neighboring nuclei. The $i_{13/2}$ neutron alignments have been observed in the $1/2^-[541]$ and $9/2^-[514]$ bands at $\hbar\omega = 0.27$ and 0.23 MeV, respectively. The difference between the crossing frequencies can be interpreted in terms of shape effects since the different proton orbits favor different nuclear shapes. There is a quite large energy splitting between the two signatures of the $9/2^-[514]$ band at low frequencies, and after the $i_{13/2}$ neutron alignment the phase of signature splitting is inverted with a much reduced amplitude. The TRS calculations show that the $9/2^-[514]$ configuration tends to have nonaxial shape with negative γ values at low frequencies, and after the $i_{13/2}$ neutron alignment the predicted positive γ deformation may cause signature inversion in the configuration of $\pi h_{11/2} \otimes \nu i_{13/2}^2$. Systematics of the signature splitting for the $9/2^-[514]$ bands at low spin in the light odd-A Re isotopes suggests that the nucleus becomes more γ soft and has larger γ deformation while decreasing the neutron number. The theoretical calculations assuming an axially symmetric nuclear shape overestimate the signature splitting in the $B(M1)/B(E2)$ ratios. Based on the unique shape (γ) dependence in the coherent influence of signature on energies and $M1$ transition matrix elements, the analysis of the available experimental data on the light Re isotopes indicates an appreciable negative γ deformation at low spins for the very neutron-deficient Re isotopes. By referring to the level structure in the nuclei around ^{169}Re, it is proposed that the three-quasiparticle band is built likely on the $\pi 9/2^-[514] \otimes \nu$AE configuration.

The authors wish to thank the staffs in the JAERI tandem accelerator for providing the ^{28}Si beam. This work was supported by the National Natural Sciences Foundation of China (grant No. 10005012), and the Major State Basic Research Development Program of China (Contract No. G2000077402). F.R. Xu acknowledges support from the National Natural Sciences Foundation of China under grant No. 10175002. Y.H. Zhang acknowledges support from NNSF (grant No. 10025525).

References

1. D.G. Roux, M.S. Fetea, E. Gueorguieva, B.R.S. Babu, R.T. Newman, J.J. Lawrie, R. Fearick, D.G. Aschman, R. Beetge, M. Benatar, G.K. Mabala, S.M. Mullins, S.H. T. Murray, S. Naguleswaran, C. Rigollet, J.F. Sharpey-Schafer, F.D. Smit, W.J. Whittaker, Phys. Rev. C **63**, 024303 (2001).
2. K. Theine, C.X. Yang, A.P. Byrne, H. Hübel, R. Chapman, D. Clarke, F. Khazaie, J.C. Lisle, J.N. Mo, J.D. Garrett, H. Ryde, Nucl. Phys. A **536**, 418 (1992).
3. C.H. Yu, M.A. Riley, J.D. Garrett, G.B. Hagemann, J. Simpson, P.D. Forsyth, A.R. Mokhtar, J.D. Morrison, B.M. Nyakó, J.F. Sharpey-Schafer, Nucl. Phys. A **489**, 477 (1988).
4. P. Frandsen, R. Chapman, J.D. Garrett, G.B. Hagemann, B. Herskind, C.H. Yu, K. Schiffer, D. Clarke, F. Khazaie, J.C. Lisle, J.N. Mo, L. Carlén, P. Ekström, H. Ryde, Nucl. Phys. A **489**, 508 (1988).
5. W. Schmitz, C.X. Yang, H. Hübel, A.P. Byrne, R. Müsseler, N. Singh, K.H. Maier, A. Kuhnert, R. Wyss, Nucl. Phys. A **539**, 112 (1992).
6. S. Jónsson, J. Lyttkens, L. Carlén, N. Roy, H. Ryde, W. Walus, J. Kownacki, G.B. Hagemann, B. Herskind, J.D. Garrett, Nucl. Phys. A **422**, 397 (1984).
7. R.A. Bark, G.D. Dracoulis, A.E. Stuchbery, A.P. Byrne, A.M. Baxter, F. Riess, P.K. Weng, Nucl. Phys. A **501**, 157 (1989).
8. H. Carlsson, M. Bergström, A. Brockstedt, L.P. Ekström, J. Lyttkens-Lindén, H. Ryde, R.A. Bark, G.B. Hagemann, J.D. Garrett, R. Chapman, D. Clarke, F. Khazaie, J.C. Lisle, J.N. Mo, Nucl. Phys. A **551**, 295 (1993).
9. L. Hildingsson, W. Klamra, Th. Lindblad, C.G. Lindén, C.A. Kalfas, S. Kossionides, C.T. Papadopoulos, R. Vlastou, J. Gizon, D. Clarke, F. Khazaie, J.N. Mo, Nucl. Phys. A **513**, 394 (1990).
10. R. Bengtsson, J.D. Garrett, *International Review of Nuclear Physics*, Vol. **2**, edited by T. Engeland, J. Rekstad, J.S. Vaagen (World Scientific, Singapore, 1989).
11. R. Bengtsson, S. Frauendorf, Nucl. Phys. A **324**, 27 (1979).
12. R. Bengtsson, S. Frauendorf, Nucl. Phys. A **327**, 139 (1979).
13. J.C. Wells, N.R. Johnson, C. Baktash, I.Y. Lee, F.K. McGowan, M.A. Riley, A. Virtanen, J. Dudek, Phys. Rev. C **40**, 725 (1989).
14. R.A. Bark, G.D. Dracoulis, A.E. Stuchbery, Nucl. Phys. A **514**, 503 (1990).
15. S. Frauendorf, F.R. May, Phys. Lett. B **125**, 245 (1983).
16. T. Kibedi, G.D. Dracoulis, B. Fabricius, A.P. Byrne, A.E. Stuchbery, Nucl. Phys. A **539**, 137 (1992).
17. V.S. Shirley, Nucl. Data Sheets **64**, 505 (1991).
18. W.D. Schmidt-Ott, H. Salewski, F. Meissner, U. Bosch-Wicke, P. Koschel, V. Kunze, R. Michaelsen, Nucl. Phys. A **545**, 646 (1992).
19. G.D. Dracoulis, B. Fabricius, T. Kibedi, A.P. Byrne, A.E. Stuchbery, A.M. Baxter, P.M. Davidson, contribution to the *International Conference on Nuclear Structure at High Angular Momentum, Ottawa, 1992* (AECL-10613, 1992) p. 36.
20. X.H. Zhou, M. Oshima, Y. Toh, Y.H. Zhang, Y. Zheng, M. Koizumi, A. Osa, T. Hayakawa, Y. Hatsukawa, T. Shizuma, M. Sugawara, Eur. Phys. J. A **15**, 285 (2002).
21. K. Furuno, M. Oshima, T. Komatsubara, K. Furutaka, T. Hayakawa, M. Kedera, Y. Hatsukawa, M. Matsuda, S. Mitarai, T. Shizuma, T. Saitoh, N. Hashimoto, H. Kusakari, M. Sugawara, T. Morikawa, Nucl. Instrum. Methods A **421**, 211 (1999).
22. S. Juutinen, P. Ahonen, J. Hattula, R. Julin, A. Pakkanen, A. Virtanen, J. Simpson, R. Chapman, D. Clarke, F. Khazaie, J. Lisle, J.N. Mo, Nucl. Phys. A **526**, 346 (1991).
23. K. Theine, A.P. Byrne, H. Hubel, M. Murzel, R. Chapman, D. Clarke, F. Khazaie, J.C. Lisle, J.N. Mo, J.D. Garrett, H. Ryde, R. Wyss, Nucl. Phys. A **548**, 71 (1992).
24. W. Nazarewicz, R. Wyss, A. Johnson, Phys. Lett. B **225**, 208 (1989).
25. W. Nazarewicz, J. Dudek, R. Bengtsson, I. Ragnarsson, Nucl. Phys. A **435**, 397 (1985).
26. W. Satula, R. Wyss, Phys. Rev. C **50**, 2888 (1994).
27. F.R. Xu, W. Satula, R. Wyss, Nucl. Phys. A **669**, 119 (2000).
28. W. Satula, R. Wyss, P. Magierski, Nucl. Phys. A **578**, 45 (1994).
29. F.R. Xu, P.M. Walker, J.A. Sheikh, R. Wyss, Phys. Lett. B **435**, 257 (1998).
30. W.F. Mueller, H.Q. Jin, J.M. Lewis, W. Reviol, L.L. Riedinger, M.P. Carpenter, C. Baktash, J.D. Garrett, N.R. Johnson, I.Y. Lee, F.K. McGowan, C.H. Yu, S. Cwiok, Phys. Rev. C **59**, 2009 (1999).
31. C.H. Yu, G.B. Hagemann, J.M. Espino, K. Furuno, J.D. Garrett, R. Chapman, D. Clarke, F. Khazaie, J.C. Lisle, J.N. Mo, M. Bergström, L. Carlén, P. Ekström, J. Lyttkens, H. Ryde, Nucl. Phys. A **511**, 157 (1990).
32. F. Dönau, S. Frauendorf, *Proceedings of the Conference on High Angular Momentum Properties of Nuclei, Oak Ridge, 1982*, edited by N.R. Johnson (Harwood Academic, New York, 1983) p. 143.
33. A.J. Larabee, L.H. Courtney, S. Frauendorf. L.L. Riedinger, J.C. Waddington, M.P. Fewell, N.R. Johnson, I.Y. Lee, F.K. McGowan, Phys. Rev. C **29**, 1934 (1984).
34. G.D. Dracoulis, G.D. Sprouse, O.C. Kistner, M.H. Rafailovich, Phys. Rev. C **29**, 1576 (1984).
35. I. Hamamoto, Nucl. Phys. A **520**, 297c (1990).
36. Y.H. Zhang, T. Hayakawa, M. Oshima, J. Katakura, Y. Hatsukawa, M. Matsuda, H. Kusakari, M. Sugawara, T. Komatsubara, K. Furuno, Phys. Rev. C **65**, 014302 (2002).
37. R.A. Bark, G.B. Hagemann, B. Herskind, H.J. Jensen, W. Korten, J. Wrzesinski, H. Carlsson, M. Bergstrom, A. Brockstedt, A. Nordlund, H. Ryde, P. Bosetti, S. Leoni, F. Ingebretsen, P.O. Tjom, Nucl. Phys. A **591**, 265 (1995).
38. W.F. Mueller, H.J. Jensen, W. Reviol, L.L. Riedinger, C.H. Yu, J.Y. Zhang, W. Nazarewicz, R. Wyss, Phys. Rev. C **50**, 1901 (1994).
39. R. Bengtsson, H. Frisk, F.R. May, J.A. Pinston, Nucl. Phys. A **415**, 189 (1984).
40. I. Hamamoto, B.R. Mottelsson, Phys. Lett. B **132**, 7 (1983).
41. F. Dönau, Nucl. Phys. A **471**, 469 (1987).
42. G.B. Hagemann, I. Hamamoto, Phys. Rev. C **40**, 2862 (1989).
43. J. Recht, Y.K. Agarwal, K.P. Blume, M. Guttormsen, H. Hübel, H. Kluge, K.H. Maier, A. Maj, N. Roy, D.J. Decman, J. Dudek, W. Nazarewicz, Nucl. Phys. A **440**, 366 (1985).
44. G.D. Dracoulis, R.A. Bark, A.E. Stuchbery, A.P. Byrne, A.M. Baxter, F. Riess, Nucl. Phys. A **486**, 414 (1988).